AEROELASTICITY AND STRUCTURAL OPTIMIZATION OF ROTOR BLADES WITH SWEPT TIPS

P.P. Friedmann* and R. Celi**
Mechanical, Aerospace and Nuclear Engineering Department
University of California
Los Angeles, California 90024-1597, U.S.A.

Abstract

A special finite element for the aeroelastic modeling of a swept tip rotor blade is derived. The swept tip of the blade is assumed to undergo moderate deflections in the flap, lag and torsional degrees of freedom. The nonlinear, partial differential equations of motion are discretized using a Galerkin type finite element method. Tip sweep introduces flap-torsion and lag-axial couplings, and may lead to aeroelastic instabilities associated with frequency coalesce. When frequency coalesce does not occur, sweep back is usually stabilizing. This aeroelastic stability and response computational capability is combined with a structural optimization analysis to minimize the n/rev vertical hub shears in forward flight, subject to aeroelastic stability and frequency placement constraints. A special technique is used to build a sequence of approximate, inexpensive to solve, optimization problems which converge to the solution of the exact problems. Tip sweep is used as an additional design variable to reduce vibration levels in forward flight.

Notation

$A(y_1,\dot{y})$	vector containing aerodynamic loads
a_g^t	vector of nodal degrees of freedom of the swept tip element in the $\hat{e}_x$, $\hat{e}_y$, $\hat{e}_z$ coordinate system
a_L^t	vector of nodal degrees of freedom of the swept tip element in the i_H, j_H, k_H coordinate system
b	blade semichord
C_T	thrust coefficient
$[C(y,\dot{y})]$	blade damping matrix
$\vec{D}$	vector of design variables
$\hat{e}_x,\hat{e}_y,\hat{e}_z$	undeformed blade coordinate system, also global coordinate system for finite element model
F	nonhomogeneous forcing vector
$f(\vec{D})$	objective function
$\nabla F(\vec{D})$	gradient of objective function or behavior constraints
$\vec{g}(\vec{D})$	vector of behavior constraints
h_s	height of the single cell cross section
$[H(\vec{D}_0)]$	Hessian of objective function or behavior constraints
h	increment for finite difference calculation of aerodynamic damping and stiffness matrices
i_H,j_H,k_H	undeformed swept tip coordinate system, also local coordinate system for the swept tip finite element
i_T,j_T,k_T	deformed swept tip coordinate system
I_b	mass moment of inertia of the blade in flapping
J	mass polar moment of inertia of the rotor
$[K(y,\dot{y})]$	blade stiffness matrix
ℓ	length of the elastic portion of the blade
ℓ_e	length of the e-th finite element used to model the blade
ℓ_t	tip length
$[M(y)]$	blade mass matrix
$[M^e],[Q^e]$	modal coordinate transformation matrix for the e-th straight finite element
$[M^t(y)]$	modal coordinate transformation matrix for the swept tip finite element
NS	number of finite elements used to model the straight portion of the blade
Q^e_{ij}	element of the modal coordinate transformation matrix $[Q^e]$ for the e-th straight finite element
R	rotor radius
R	position vector of a point of the swept tip
t_1	thickness of the cross section
u	axial elastic displacement
v,w	bending elastic displacements in the direction of j_H and k_H
V_{zpk}	peak-to-peak value of the 4/rev vertical hub shears, nondimensionalized through division by $2\Omega^2 I_b/\ell$

* Professor and Chairman
** Currently Assistant Professor, Aerospace Engineering Department, University of Maryland, College Park, MD.

x_A offset between the elastic axis and the aerodynamic center, positive for aerodynamic center ahead of the elastic axis

x_I offset between the elastic axis and the center of gravity, positive for center of gravity ahead of the elastc axis.

x_1 distance between leading edge and internal wall in double cell cross section

x_2 chordwise length of the cross section

x_0 tip spanwise coordinate, measured along the i_H axis starting from the junction with the straight portion of the blade

x_j spanwise position of the junction, measured from the blade root

y vector of generalized coordinates of the blade

y_0, z_0 cross sectional coordinates of a point on the swept tip, measured along j_T and k_T respectively

β_p precone angle of the blade

γ blade lock number

ζ_k real part of hover stability eigenvalue for the k-th mode

Λ tip sweep angle, positive for backward sweep

μ advance ratio

σ rotor solidity

ρ mass density of the blade

ϕ elastic torsional rotation of the swept tip

Ω angular velocity vector of the rotor

Ω rotor angular velocity

ψ Azimuth angle

$(\dot{})$ derivative w.r.t. time

I. Introduction and Problem Statement

During the last few years, rotor blades with tip planform shapes other than rectangular have received considerable attention. Tip sweep and taper play an important role in alleviating both compressibility effects on the advancing blade and stall effects on the retreating blade. In addition, they help reduce aerodynamic noise, and have the potential for "tailoring" the aeroelastic response of the blade.

Several investigators have studied recently the aerodynamic characteristics of swept tips [1-3]. These studies seem to indicate that careful dynamic and aeroelastic modeling of the blade is a prerequisite for accurate aerodynamic calculations. In fact, swept tips introduce powerful bending-torsion coupling effects which significantly influence blade dynamics, because they operate in regions of high dynamic pressure and of relatively large elastic displacements. This statement is applicable to both articulated as well as hingeless and bearingless rotor blades.

The modeling of the dynamic effects introduced in a rotor blade by sweep is a complicated aeroelastic stability and response problem. Therefore, only limited information on the effect of tip sweep on the dynamics of helicopter rotor blades is presently available. One of the earliest systematic, analytical studies is due to Tarzanin and Vlaminck (Ref. 4), who studied the effect of tip sweep on the hub loads of an articulated rotor system. The mathematical model consisted of coupled flap-torsion, and uncoupled lag equations of motion. A Myklestad type solution technique was used. A number of interesting conclusions regarding the effect of sweep were obtained: (1) sweep is not beneficial for all rotor blades; (2) there is no optimal sweep angle for all airspeeds; (3) blade properties, and in particular torsional stiffness, may drastically influence the effect of tip sweep; and (4) improved analytical models are needed for a better fundamental understanding of the dynamics of blades with swept tips.

Current mathematical models of swept tips are based on approximate modifications of straight blade models [4]. Typically, sweep is simulated by manipulating the relative positions of aerodynamic center, center of gravity, and shear center of the cross sections. More refined theories, capable of modeling helicopter blades with curved undeformed elastic axes have become available recently, and are reviewed in Ref. 5. Among these, the theory developed by Rosen and Rand [6,7] contains some of the ingredients required to model rotor blades with swept tips; however, this model was never used to model rotor blades with swept tips, due to its somewhat cumbersome mathematical form.

Another recent study [8] has emphasized the use of blade sweep as a means for reducing 4/rev hub loads, using a modified version of the analysis presented in Ref. 4. The experimental and theoretical study of coupled flap-pitch flutter for a swept tip, composite bearingless rotor blade in hover was presented in Ref. 9. The mathematical details of the analytical model were not presented in Ref. 9. The agreement between the theory and experiment was incomplete and it is not evident from Ref. 9 that a satisfactory mathematical model for the aeroelastic behavior of swept tip rotors has been derived.

From this brief review of the pertinent literature, it is evident that there is a strong need for a consistent aeroelastic model capable of simulating the dynamic behavior of rotor blades with swept tips. It is also important to note that this is both an important practical problem for the helicopter industry as well as a fundamental, and quite complex, theoretical problem which has received only very limited attention in the past. The general objective of this article is to remedy this situation by presenting a finite element model capable of simulating the aeroelastic behavior of swept tip helicopter blades in both hover and forward flight.

Furthermore the influence of sweep on both aeroelastic response and stability is a powerful effect and it is natural to raise the question

about the possible use of blade tip sweep as a design variable in a structural optimization process aimed at vibration reduction in forward flight. Such a structural optimization approach to the vibration reduction problem implies that the design problem is cast in mathematical programming form and the blade mass and stiffness distributions and its geometry are determined, by the optimizer, in such a manner that the vibration levels at the rotor hub are minimized. Recent surveys [10,11] on the use of modern structural optimization for vibration reduction in rotorcraft reveal the existence of a very limited body of work where blade vibration levels are reduced while simultaneously satsifying the aeroelastic constraints imposed on the blade.

A serious problem encountered in the direct coupling of a comprehensive aeroelastic stability and response analysis code with an optimization, or nonlinear mathematical programming code is the very large computational effort required for the solution. This problem can be alleviated by constructing an approximate, computationally easier to solve, optimization problem [12]. The approximate problem is updated frequently, so that the sequence of solutions of the approximate problems converges to the solution of the original, exact optimization problems.

In a previous study [13] an expensive approach, based on finite differences for generating approximations to the objective function and aeroelastic constraints was used. The generation of the approximate problem was cumbersome and it had to be carried out in an interactive manner during the optimization process. In this paper a more effective method for dealing with this problem is presented.

The specific objectives of this paper are:

1. To present a new mathematical model for the aeroelastic behavior of a helicopter rotor blade with a swept tip. This is accomplished by deriving a special finite element model for the swept tip, which accounts for the effects of sweep on the inertia, aerodynamic, and structural operators associated with this aeroelastic problem. The formulation is valid for arbitrary sweep angles, and accounts for general variations of mass, stiffness, and geometric properties of the blade in the tip region.

2. To gain a fundamental understanding of the influence of sweep on the aerelastic response and stabiilty of hingeless rotor blades in hover and forward flight. This is accomplished by presenting results illustrating the effect of tip sweep on the aeroelastic response and stability of an isolated, hingeless rotor blade.

3. To present a new formulation of the structural optimization problem, for a helicopter rotor blade in forward flight. The objective is the minimization of the n/rev vertical hub shears. The behavior constraints express mathematically the requirements that the blade be aeroelastically stable, that its natural frequencies fall between preassigned upper and lower bounds, and that the autorotation performance not be degraded during the aeroelastic tailoring process. A new formulation of the approximate problem allows increases in efficiency, in the complete solution of the optimum design problem of at least one order of magnitude, compared with existing procedures.

4. To present results obtained by letting the tip sweep angle be one of the design variables in the optimization procedure. Tip sweep has a powerful influence on the dynamic behavior of the blade, and when included in the aeroelastic tailoring process, can lead to further reductions in blade vibration levels.

II. Aeroelastic Stability and Response Analysis

The geometry of the problem is shown in Fig. 1. The assumptions made in derivation of the structural and inertia operator for the swept tip are similar to those used in Ref. 14 to derive the equations of motion of a straight blade. In particular, Bernoulli-Euler beam theory applies; the swept tip undergoes moderate deflections, which implies small strains and finite rotations or slopes, the elastic torsional deformations occur about the undeformed elastic axis, and additional torsional deformations may occur at the blade root, due to the flexibility of the control system; the blades are attached to an aircraft of infinite mass, thus no coupling between the fuselage and the blade dynamics exists; the helicopter is in trimmed, steady, and straight flight.

The elastic axis of the blade is defined as the line connecting the shear centers of the cross sections of the blade. Therefore the elastic axis is composed of two straight segments, namely the elastic axis of the straight portion of the blade and the elastic axis of the swept tip. A force applied at a point on the elastic axis of the swept tip will produce only a bending moment within the tip portion, and no torsional elastic deformations of the tip region will occur. At the junction with the straight portion of the blade, however, a component of this bending moment will become a torsional moment for the straight portion, and torsional deformations of the straight portion will occur.

Two-dimensional, quasi-steady aerodynamics is used for the representation of the aerodynamic loads. Stall and compressibility effects are neglected, since the main objective of this study is to examine the basic effect of sweep on the aeroelastic behavior. The independence principle is assumed to apply; that is, the aerodynamic loads depend only on the component of the flow contained in the plane of the cross-section (the $j_T - k_T$ plane), and radial flow effects are neglected. Although the aerodynamic model is essentially the same as in Ref. 14, a new, substantially different implementation is used. The algebraic expressions that define the aerodynamic loads are not expanded explicitly. They are coded separately in a computer program, and combined numerically during the solution procedure. Thus, the aerodynamic loads do not appear in the equations of motion as explicit functions of the blade displacements. Rather, they appear as general forcing terms, the numeric value of which is introduced into the equations of motion when the stability and response problem is

solved. The new, implicit formulation is used for the aerodynamic modeling of both the straight and the swept portions of the blade. A more detailed description of its implementation, and of its numerical properties, can be found in Ref. 15.

A basic ingredient for the formulation of the equations of motion is the position vector R of a generic point P on the swept tip, which is given by

$$\mathbf{R} = e_1\mathbf{i} + x_j\hat{\mathbf{e}}_x + (x_0 + u)\,\mathbf{i}_H + v\mathbf{j}_H + w\mathbf{k}_H + y_0\mathbf{j}_T + z_0\mathbf{k}_T \qquad (1)$$

The coordinate system $\mathbf{i}_H$, $\mathbf{j}_H$, $\mathbf{k}_H$ is the undeformed swept tip coordinate system obtained from the undeformed blade coordinate system $\hat{\mathbf{e}}_x$, $\hat{\mathbf{e}}_y$, $\hat{\mathbf{e}}_z$ through a rotation about $\hat{\mathbf{e}}_x$ axis of the sweep angle Λ. The coordinate system $\mathbf{i}_T$, $\mathbf{j}_T$, $\mathbf{k}_T$ is the deformed tip coordinate system. For zero sweep angle, the unit vectors $\mathbf{i}_H$, $\mathbf{j}_H$, $\mathbf{k}_H$ coincide with the $\hat{\mathbf{e}}_x$, $\hat{\mathbf{e}}_y$, $\hat{\mathbf{e}}_z$. Then Eq. (1) provides the position vector of a point P on the unswept portion of the blade when written in the form:

$$\mathbf{R} = e_1\mathbf{i} + (x_p + u)\hat{\mathbf{e}}_x + v\hat{\mathbf{e}}_y + w\hat{\mathbf{e}}_z + y_0\mathbf{j}_T + z_0\mathbf{k}_T \qquad (2)$$

where x_p is the spanwise coordinate of P. The coordinate system transformation between $\mathbf{i}_T$, $\mathbf{j}_T$, $\mathbf{k}_T$ system and the $\mathbf{i}_H$, $\mathbf{j}_H$, $\mathbf{k}_H$ system is based on the assumption of moderate blade displacements and small strains, and is given by (Ref. 14).

$$\begin{Bmatrix}\mathbf{i}_T\\ \mathbf{j}_T\\ \mathbf{k}_T\end{Bmatrix} = \begin{bmatrix} 1 & v_{,x} & w_{,x} \\ -(v_{,x}+\phi w_{,x}) & 1 & \phi \\ -(w_{,x}-\phi v_{,x}) & -(\phi+v_{,x}w_{,x}) & 1 \end{bmatrix} \begin{Bmatrix}\mathbf{i}_H\\ \mathbf{j}_H\\ \mathbf{k}_H\end{Bmatrix} \qquad (3)$$

After performing the appropriate coordinate transformations, Eq. (1) becomes:

$$\mathbf{R} = [(x_j + e_1)\cos\Lambda + x_0 - u - y_0(v_{,x} + \phi w_{,x}) - z_0(w_{,x} - \phi v_{,x})]\mathbf{i}_H + [(x_j + e_1)\sin\Lambda + v + y_0 + z_0(\phi + v_{,x}w_{,x})]\mathbf{j}_H + [w - \beta_p e_1 + y_0\phi + z_0]\mathbf{k}_H \qquad (4)$$

The angular velocity vector $\boldsymbol{\Omega}$ is given by:

$$\boldsymbol{\Omega} = \Omega\mathbf{k} = \Omega(\beta_p\cos\Lambda\,\mathbf{i}_H + \beta_p\sin\Lambda\,\mathbf{j}_H + \mathbf{k}_H) \qquad (5)$$

The distributed inertia load vector $\mathbf{p}_I$, and the distributed inertia moment vector $\mathbf{q}_I$ are respectively given by:

$$\mathbf{p}_I = p_{xI}\mathbf{i}_H + p_{yI}\mathbf{j}_H + p_{zI}\mathbf{k}_H = -\int_A \rho\,\mathbf{a}\,dA \qquad (6)$$

$$\mathbf{q}_I = q_{xI}\mathbf{i}_H + q_{yI}\mathbf{j}_H + q_{zI}\mathbf{k}_H = -\int_A \rho(y_0\mathbf{j}_T + z_0\mathbf{k}_T)\times\mathbf{a}\,dA \qquad (7)$$

where $\mathbf{a}$ is the vector acceleration of the point on the swept tip, given by

$$\mathbf{a} = \mathbf{R} + 2(\boldsymbol{\Omega}\times\mathbf{R}) + \boldsymbol{\Omega}\times(\boldsymbol{\Omega}\times\mathbf{R}) \qquad (8)$$

The algebraic manipulations associated with Eqs. (6) and (7) produce expressions of considerable length. These expressions are omitted in this paper for brevity. They can be found in Ref. 15, together with the complete equations of motion of the swept tip.

The spatial dependence of the nonlinear, partial differential equations of motion of the swept tip is discretized using a local Galerkin method of weighted residuals, resulting in a finite element formulation. Flap bending is modeled using four degrees of freedom, namely displacement and rotation at each end of the tip element, and cubic Hermite interpolation polynomials. Lag bending is modeled in the same way. Torsion is modeled using three degrees of freedom, namely the rotations at each end of the tip element and at its mid-point, and quadratic Hermite interpolation polynomials. This choice of interpolation polyomials defines the simplest element which yields a consistent formulation for coupled bending and torsion. The interpolation polynomials are the same as those used in Ref. 17.

The axial degree of freedom is elminated by making the assumption that the blade is inextensional in the axial direction, which gives:

$$u = -\frac{1}{2}\int_{\ell}(v_{,x}^2 + w_{,x}^2)\,d\vec{\ell} \qquad (9)$$

in which $\vec{\ell}$ is a vector tangent to the elastic axis of the blade.

The equations of motion for the swept tip are derived in the preconed, swept, undeformed coordinate system $\mathbf{i}_H$, $\mathbf{j}_H$, $\mathbf{k}_H$, shown in Fig. 1. This is also the local coordinate system for the swept tip element. The preconed, undeformed, straight blade coordinate system $\hat{\mathbf{e}}_x$, $\hat{\mathbf{e}}_y$, $\hat{\mathbf{e}}_z$, shown in Fig. 1, is the global coordinate system for the finite element model of the complete blade. The local-to-global coordinate transformation can be written in the form:

$$\mathbf{a}_L^t = [\Lambda]\mathbf{a}_G^t \qquad (10)$$

The vectors $\mathbf{a}_L^t$ and $\mathbf{a}_G^t$ are the vectors of nodal degrees of freedom of the swept tip element, in the local and global coordinate system respectively, and are defined as follows:

$$\mathbf{a}_L^t = [v_1\ v_{,x_1}\ v_2\ v_{,x_2}\ w_1\ w_{,x_1}\ w_2\ w_{,x_2}\ \phi_1\ \phi_2\ \phi_3]^T \qquad (11)$$

$$\mathbf{a}_G^t = [v_J\ v_{,x_J}\ v_T\ v_{,x_T}\ w_J\ w_{,x_J}\ w_T\ w_{,x_T}\ \phi_J\ \phi_M\ \phi_T\ u_J]^T \qquad (12)$$

The various components of $\mathbf{a}_L^t$ and $\mathbf{a}_G^t$ are shown in Figs. 2 and 3, respectively. Although the axial

displacement u_j of the junction section appears explicitly in the vector a_G^t, the axial degree of freedom will not be retained as an independent degree of freedom in the solution of the equations of motion. The axial displacement is eliminated by making the assumption that the blade is inextensional, and u_j appears temporarily in Eq. (12) for convenience of implementation. Equation (10) is an approximate coordinate transformation, based on a small deflection assumption which implies that elastic rotations can be expressed as vectors. A coordinate transformation consistent with the moderate deflections assumption has been presented in Ref. 18. Numerical results presented in Ref. 18 confirm that the nonlinear terms omitted in Eq. (10), due to the moderate deflections are negligible for the range of tip sweep angles considered in this study.

In general, the powerful effects of tip sweep on blade stability and response, which are evident from the results presented in the following sections, will not be modified by the approximations introduced which are associated with higher order effects, such as those due to moderate deflections.

The local-to-global coordinate transformation matrix $[\Lambda]$ is defined as follows:

$$[\Lambda] = \begin{bmatrix} [\Lambda_{LL}] & 0 & 0 & \{\Lambda_{LA}\} \\ 0 & [\Lambda_{FF}] & [\Lambda_{FT}] & 0 \\ 0 & [\Lambda_{TF}] & [\Lambda_{TT}] & 0 \end{bmatrix} \qquad (13)$$

The nonzero submatrices in Eq. (13) are given below:

$$[\Lambda_{LL}] = \begin{bmatrix} \cos\Lambda & 0 & 0 & 0 \\ 0 & 1 & 0 & 0 \\ -\frac{\sin^2\Lambda}{\cos\Lambda} & 0 & \frac{1}{\cos\Lambda} & 0 \\ 0 & 0 & 0 & 1 \end{bmatrix}$$

$$[\Lambda_{FF}] = \begin{bmatrix} 1 & 0 & 0 & 0 \\ 0 & \cos\Lambda & 0 & 0 \\ 0 & 0 & 1 & 0 \\ 0 & 0 & 0 & \cos\Lambda \end{bmatrix}$$

$$[\Lambda_{FT}] = \begin{bmatrix} 0 & 0 & 0 \\ -\sin\Lambda & 0 & 0 \\ 0 & 0 & -\sin\Lambda \\ 0 & 0 & 0 \end{bmatrix}$$

$$[\Lambda_{TF}] = \begin{bmatrix} 0 & \sin\Lambda & 0 & 0 \\ 0 & \frac{1}{2}\sin\Lambda & 0 & \frac{1}{2}\sin\Lambda \\ 0 & 0 & 0 & \sin\Lambda \end{bmatrix}$$

$$[\Lambda_{TT}] = \begin{bmatrix} \cos\Lambda & 0 & 0 \\ 0 & \cos\Lambda & 0 \\ 0 & 0 & \cos\Lambda \end{bmatrix} ; \quad \{\Lambda_{LA}\} = \begin{Bmatrix} \sin\Lambda \\ 0 \\ \sin\Lambda \\ 0 \end{Bmatrix}$$

The submatrices $[\Lambda_{LL}]$ and $\{\Lambda_{LA}\}$ are derived by making the assumption that the tip is axially rigid, and thus $u_1 = u_2$. This assumption is not used anywhere else in this study, and the primary reason for its use here is to facilitate the elimination of the axial displacement u_T. The submatrix $[\Lambda_{TF}]$ is obtained by making the asusmption that the slope $w_{,x}$ at the mid-element node is the average of the slopes at the two ends of the element. This assumption is required because the element has a mid-element node for the modeling of torsion, but not for the modeling of bending.

Equation (13) clearly shows that a swept tip introduces two types of coupling, namely flap-torsion coupling, and lag-axial coupling. Because of the assumption of inextensibility, the axial degree of freedom is a nonlinear function of the bending degrees of freedom. Therefore, if such an assumption is made, the lag-axial coupling becomes a nonlinear effect. In this study, the calculation of the natural frequencies and mode shapes of the blade is assumed to be a linear problem; therefore, for such calculations, a slightly different form of $[\Lambda]$ is used with the submatrix $\{\Lambda_{LA}\}$ set equal to zero.

As a preliminary step before the solution of the equations of motion for both, hover and forward flight, a modal coordinate transformation is performed. The purpose of the transformation is twofold; to reduce the number of unknowns of the problem, representing the nodal degrees of freedom of the blade, and to assemble the various element matrices into the system mass, damping, and stiffness matrices, and into the system load vectors. For the swept tip element, the modal coordinate transformation has the form:

$$a_G^t = [M^t(y)\ y] \qquad (14)$$

The vector y is the vector of generalized coordinates, which become the new unknowns of the problem. If m modes are used to perform the modal coordinate transformation, then y is a vector of size m. The modal coordinate transformation has the form:

$$[M^t(y)] = \begin{bmatrix} [Q_t] \\ \hline U^T(y) \end{bmatrix} \qquad (15)$$

The submatrix $[Q_t]$ is a matrix of size 11 by m, the columns of which contain the portions of the normal mode eigenvectors corresponding to the swept tip. The modes used in the coordinate transformation are coupled, rotating normal modes, computed for a root pitch angle equal to the collective pitch. $U^T(y)$ is a row vector of size m, the i-th element of which is given by:

$$U_i(y) = -\frac{1}{2}\sum_{e-1}^{NS}\sum_{j=1}^{m} y_j \cdot \sum_{k=1}^{4}\sum_{\ell=1}^{4}\left(Q^e_{ik}Q^e_{j\ell}\int_0^{\ell_e} \gamma_{,x_k}\,\gamma_{,x_\ell}\,dx_e + Q^e_{i,k+4}Q^e_{j,\ell+4}\int_0^{\ell_e}\eta_{,x_k}\,\eta_{,x_\ell}\,dx_e\right) \quad (16)$$

$U^T(y)$ is associated with the inextensibility assumption. In fact, the axial displacement u_J of the junction section can be written in the form:

$$u_J = -\frac{1}{2}\int_0^{x_j}\left(v^2_{,x} + w^2_{,x}\right)dx = U^T(y)\cdot y \quad (17)$$

where x_j is the spanwise coordinate of the junction section. In Eq. (16), $\gamma_{,xk}$ and $\eta_{,xk}$ represent the derivatives with respect to x of each of the four interpolation polynomials used in the modeling of bending [Ref. 16].

The modal coordinate transformation matrix $[M^e]$ for the straight elements of the blade is a matrix of size 11 by m, obtained from Eq. (15) by dropping the last row, that is:

$$[M^e] = [Q^e] \quad (18)$$

(the superscript "e" denotes a straight element, consistent with the notation of Ref. [17]). An important difference between the modal coordinate transformations for a straight element and for a swept tip element is that latter is nonlinear, and depends on the equilibrium position of the blade. The nonlinearity is due to the inextensibility assumption and appears due to of the axial-lag coupling introduced by the swept tip.

The stiffness matrix $[K(y,\dot{y})]$ of the complete blade is assembled by summing the stiffness matrices of the individual elements, after the modal coordinate transformation has been performed on each of them, that is:

$$[K(y)] = \sum_{e=1}^{NS}[M^e]^T[K^e(y,\dot{y})][M^e] + [M^t(y)]^T[\Lambda]^T[K^t(y,\dot{y})][\Lambda][M^t(y)] \quad (19)$$

where $[K^e(y)]$ is the stiffness matrix of the e-th straight finite element, and $[K^t(y)]$ is the stiffness matrix of the swept tip element, in the tip local coordinate system. The blade mass matrix $[M(y)]$, damping matrix $[C(y)]$, aerodynamic load vector $A(y)$, and the nonhomogeneous load vector F, are assembled in a similar manner.

The final equations of motion are a set of nonlinear, coupled, ordinary differential equations, which can be written in the form:

$$[M(y)]\ddot{y} + [C(y,\dot{y})]\dot{y} + [K(y,\dot{y})]y + A(y,\dot{y}) + F = 0 \quad (20)$$

For the general case of forward flight, these equations also have periodic coefficients. In Eq. (20) the matrices M, C, and K contain inertia and structural terms, but not the aerodynamic terms, which are all contained in the vector A.

For the case of hover, and within the assumptions used in this study, the nonlinear equations have constant coefficients. The generalized coordinate vector y is then written as the sum of a constant vector y_0 and a perturbation, time dependent vector $\Delta y(t)$:

$$y = y_0 + \Delta y(t) \quad (21)$$

Substitution of Eq. (21) into Eq. (20) leads to a system of nonlinear algebraic equations:

$$[K(y_0,0)]y_0 + A(y_0,0) + F = 0 \quad (22)$$

and to a system of small perturbation, linear ordinary differential equations of motion:

$$[M(y_0)]\Delta\ddot{y} + [\bar{C}(y_0,0)]\Delta\dot{y} + [\bar{K}(y_0,0)]\Delta y = 0 \quad (23)$$

with

$$[\bar{C}(y_0,0)] = [C(y_0,0)] + \left[\frac{\partial A}{\partial \dot{y}}\right]_{\substack{y=y_0\\ \dot{y}=0}} \quad (24)$$

$$[\bar{K}(y_0,0)] = [K(y_0,0)] + \sum_{i=1}^{m}\left.\frac{\partial[K(y,\dot{y})]}{\partial y_i}\right|_{\substack{y=y_0\\ \dot{y}=0}} y_{0_i} + \left[\frac{\partial A}{\partial y}\right]_{\substack{y=y_0\\ \dot{y}=0}} \quad (25)$$

Since the numerical value of the aerodynamic load vector A is known as a function of y and $\dot{y}$ the aerodynamic stiffness and damping matrices $\left[\frac{\partial A}{\partial y}\right]$ and $\left[\frac{\partial A}{\partial \dot{y}}\right]$ which appear in Eqs. (24) and (25) are computed numerically using finite difference approximations. The i-th column of $\left[\frac{\partial A}{\partial y}\right]$ for $y = y_0$ and $\dot{y} = 0$ is given by:

$$\left\{\frac{\partial A}{\partial y_i}\right\} \cong \frac{A(y_0 + h,0) - A(y_0,0)}{h} \quad (26)$$

in which h is a vector with all its elements equal to zero, except for the i-th which is equal to h. Similarly, the i-th column of $\left[\frac{\partial A}{\partial \dot{y}}\right]$ for $y = y$ and $\dot{y} = 0$ is given by

$$\left\{\frac{\partial A}{\partial \dot{y}_i}\right\} \cong \frac{A(y_0 + h,0) - A(y_0,0)}{h} \quad (27)$$

Equation (22) is solved using a Newton-Raphson iteration procedure. The solution vector y_0 represents the static nonlinear equilibrium

position of the blade in hover. The linearized stability is determined from Eq. (23), by solving a standard eigenvalue problem.

In forward flight, the equilibrium position is time dependent and is obtained by solving a sequence of linear, periodic response problems, using quasilinearization (Ref. 19). The stability of the system is determined using Floquet theory. A detailed description of the solution procedure, including the special treatment of the aerodynamic loads, is presented in Ref. 15.

III. Formulation of the Optimum Design Problem

The optimization problem is cast in nonlinear mathematical programming form. Thus the objective is to minimize a function $f(\vec{D})$ of a vector $\vec{D}$ of design variables, subject to a certain number of constraints $\vec{g}(\vec{D}) \leq 0$:

$$\text{minimize } f(\vec{D}) \tag{28}$$

subject to:

$$\vec{g}(\vec{D}) \leq 0 \tag{29}$$

As indicated in Section I the structural optimization will be realistic only if the aeroelastic constraints are retained in Eq. (29). Some recent work has addressed the minimum weight design of rotor blades with frequency constraints [20] as well as the vibration reduction problem in forward flight by using optimally placed tuning masses [21] without enforcing aeroelastic stability constraints and without using an aeroelastic response analysis to obtain the vibratory loads. While such studies are useful since they contribute towards the overall understanding of the problem they do not produce reliable designs, as indicated by a very detailed study which was aimed at a experimental verification of helicopter blade designs optimized for vibration reduction [22].

To reduce the computational requirements, the computer program performing the aeroelastic analysis is not connected directly to the optimization program. Instead, the optimization is conducted on an approximate problem, which reproduces the characteristics of the actual problem in a neighborhood of the current design, and which is continuously updated as the optimization progresses.

An effective method of building an approximate problem is to expand the objective function and the behavior constraints in Taylor series in terms of the design variables [12]:

$$F(\vec{D}) \approx F(\vec{D}_o) + \nabla F(\vec{D}_0)\delta\vec{D} + \frac{1}{2}\delta\vec{D}^T[H(\vec{D}_0)]\delta\vec{D} \tag{30}$$

where $F(\vec{D})$ is taken to be any objective or constraint function, $\vec{D}_0$ is the current design, and $\nabla F(\vec{D}_0)$ and $[H(\vec{D}_0)]$ are respectively the gradient and the Hessian matrix at the current design. The Hessian matrix is the matrix of the second partial derivatives of the objective function with respect to the design variables. The perturbation vector $\delta\vec{D}$ is defined as:

$$\delta\vec{D} = \vec{D} - \vec{D}_0 \tag{31}$$

The most expensive function to evaluate is the objective function. The cost of one evaluation of the objective function is two orders of magnitude higher than the total cost of evaluating the behavior constraints. No analytic expressions for the gradients are available for the objective function, and finite difference approximations are required for the construction of the derivative information in Eq. (30). Therefore, if n design variables are used in the optimization, n additional aeroelastic analyses are required to compute the gradient, and an additional n(n+1)/2 for the calculation of the Hessian, making the cost of building the Taylor series approximation of the objective function extremely high. For this reason an alternative approximation technique, introduced by Vanderplaats [23,24], was used in this study.

This alternative technique is based on the idea of approximating the gradient and the Hessian in Eq. (30), not by using small finite difference steps, but by using whatever design information is available at the time. Equation (30) can be rewritten, in expanded form, as [23,24]

$$\begin{aligned}\Delta F = {} & \nabla F_1\delta D_1 + \nabla F_2\delta D_2 + \ldots + \nabla F_n\delta D_n \\ & + \tfrac{1}{2}(H_{11}\delta D_1^2 + H_{22}\delta D_2^2 + \ldots + H_{NN}\delta D_n^2) \\ & + H_{12}\delta D_1\delta D_2 + H_{13}\delta D_1\delta D_3 + \ldots + H_{1n}\delta D_1\delta D_n \\ & + H_{23}\delta D_2\delta D_3 + \ldots + H_{n-1,n}\delta D_{n-1}\delta D_n\end{aligned} \tag{32}$$

where

$$\Delta F = F(\vec{D}) - F(\vec{D}_0) = F - F_0 \tag{33}$$

and

$$\Delta F_i = \nabla F_i(\vec{D}_0) \;;\; H_{ij} = H_{ij}(\vec{D}_0) \tag{34}$$

Assume that a baseline design $\vec{D}_0$ has been analyzed to give F_0, and that other designs $\vec{D}_1, \vec{D}_2, \ldots, \vec{D}_k$ have been previously analyzed, to provide $F_1, F_2, \ldots, F_k$. Let

$$\delta\vec{D}_i = \vec{D}_i - \vec{D}_0 \qquad i = 1,2,..,k \tag{35}$$

and

$$\Delta F_i = F_i - F_0 \qquad i = 1,2,\ldots,k \tag{36}$$

If k designs are available, Eq. (32) can be written k times. The unknowns of the resulting linear system are $\nabla F_1, \nabla F_2, \ldots, \nabla F_k$, and $H_{11}, H_{12}, \ldots, H_{nn}$. If exactly $l = 1 + n + n(n+1)/2$ designs are available and if all the designs are linearly independent, the system of l equations (32) will provide all the coefficients required for the quadratic polynomial approximation Eq. (30). If all the designs are very closely spaced, the solution of

the system of Eqs. (32) will provide the finite difference approximations to gradient and Hessian matrix at $\vec{D}_0$. Equation (30) will then represent a truncated Taylor series expansion of F, valid in a neighborhood of $\vec{D}_0$. If the designs are dispersed in the design space, Eq. (30) will simply be a quadratic polynomial approximation, defined over a wider region of the design space.

An important characteristic of this technique is that the system of Eqs. (32) can be written with less than 1 equations. If at least n+1 designs are available, the solution of the system will provide the linear portion of the approximation, Eq. (30). An approximate optimization can be conducted, based on this linear approximation. The resulting optimum is then analyzed precisely, and provides an additional design: a system of n+2 equations (32) can then be written. Its solution will provide a new approximation, Eq. (32), with all the linear terms plus one pair of quadratic terms of the symmetric Hessian matrix. The process can then be repeated, with each new approximate optimum providing an additional design point to increase the number of terms in the quadratic approximation to objective function and behavior constraints.

One iteration of the optimum design process thus consists of the follwing 6 steps:

1. Calculation of the blade properties, including natural frequencies and mode shapes;
2. Aeroelastic analysis in hover;
3. Aeroelastic analysis in forward flight, including calculation of hub loads;
4. Calculation of objective function and behavior constraints;
5. Calculation of a new approximation (linear or incomplete quadratic) to objective function and behavior constraints;
6. Solution of the approximate constrained optimization problem, using the feasible direction code CONMIN [25], to obtain a new, improved blade design.

The process is terminated when a feasible, optimum design has been reached, or arbitrarily, when the improvement in the design is considered "adequate".

The first n+1 iterations of the procedure are not true optimization iterations, because Steps 5 and 6 above are not performed. In fact, these initial iterations are used to generate a sufficient number of designs, to build at least an initial linear approximation to objective function and behavior constraints.

Side constraints are placed on the design variables, to prevent them from reaching impractical values which violate practical, physical constraints. Thus all the thicknesses and distances are assumed to be nonnegative numbers. No side constraints were placed on the tip sweep angle Λ, which could assume positive (swept back tip) or negative angles, as determined by the optimizer.

Three different types of behavior constraints are placed on the design:

1. Frequency placement constraints. The fundamental frequencies in flap, lag and torsion are required to fall between preassigned upper and lower bounds. It ω is one of the three frequencies, and ω_L and ω_U are the preassigned lower and upper bound respectively, the frequency placement constraints are expressed mathematically in the form:

$$g(\vec{D}) = \frac{\omega^2}{\omega_U^2} - 1 \leq 0 \qquad (37)$$

$$g(\vec{D}) = 1 - \frac{\omega^2}{\omega_L^2} - 1 \leq 0 \qquad (38)$$

Equations (37) and (38), written for each of the three fundamental frequencies of the blade, provide a total of six behavior constraints. Furthermore the frequencies are also constrained so as to be sufficiently removed from the n/rev frequencies.

2. Aeroelastic stability constraints. The blade is required to be aeroelastically stable in hover. No constraints are placed on the stability in forward flight, because all the blade configurations considered in this optimization study are soft-in-plane blade configurations, and the effect of forward flight is usually stabilizing for this type of blades [19]. The aeroelastic stability constraints are expressed mathematically in the form:

$$g(\vec{D}) = \zeta_k \leq 0 \qquad k = 1,2,\ldots m \qquad (39)$$

If m modes are used to perform the modal coordinate transformation in the solution of the equations of motion, there are m constraint equations like Eq. (39), where the quantity ζ_k is the real part of the hover stability eigenvalue for the k-th mode.

3. Autorotation constraints. The autorotation constraint expresses the requirement that possible mass redistributions produced in the optimization process do not degrade autorotation properties of the rotor. The most important measure of the autorotation properties of a rotor is the mass polar moment of inertia of the rotor [26]. Therefore the autorotation constraint is expressed mathematically in the form:

$$g(\vec{D}) = 1 - \frac{J}{0.9J_0} \leq 0 \qquad (40)$$

The constraint equation (40) requires that the mass polar moment of inertia J of the rotor maintain, during the optimization, at least 90% of its initial value J_0.

Therefore, a total of thirteen behavior constraint equations are placed on the design variables.

IV. Results

IV.1 Aeroelastic Behavior of Swept Tip Rotors

Two basic blade configurations were considered for the forward flight study: a soft-in-plane and a stiff-in-plane hingeless blade configuration, with uncoupled fundamental lag frequencies of 0.732/rev and 1.42/rev, respectively. For both configurations, the uncoupled fundamental flap and torsion frequencies for zero sweep were 1.125/rev and 3.17/rev, respectively. The Lock number was $\gamma = 5.5$, the thrust coefficient $C_T = 0.005$, and the rotor solidity $\sigma = 0.07$. Only selected results are presented in this paper additional results can be found in Refs. 16 and 27.

The aeroelastic stability of the swept tip rotor blade in hover is illustrated in Fig. 4 for a collective pitch setting of $\theta_0 = 0.1432$. The 0.10R outboard portion of the blade is gradually swept back. The combined effects of sweep and precone are shown in the figure. Precone interacts with sweep to change the nose-down torsional moment due to lift and the nose up moment due to centrifugal force. The influence of sweep and precone on the root-locus of first torsion and first lag mode are presented in Fig. 4. For zero precone frequency coalesce occurs between the first lag and first torsion mode. As frequencies coalesce, the torsional damping increases considerably, while the lag mode becomes unstable. This lag instability is not eliminated by small amount of structural damping [28] indicating that this is a strong instability. For $\beta_p = 3°$, increasing sweep increases the imaginary part of the first torsion eigenvalue, instead of decreasing it, as was the case for zero precone. Thus frequency coalesce does not occur, and the lag mode remains stable. Numerous additional results, for the case of hover, can be found in Refs. 16 and 27.

Tip sweep has also an important influence of the aeroelastic stability in forward flight. Figure 5 shows the real part of the characteristic exponent of the first lag mode, as a function of advance ratio, for the stiff-in-plane configuration considered in the previous plot. For the blades with the swept tip, forward flight is stabilizing; and no instabilities are encountered in the range of advance ratios considered. In the absence of sweep, the real part of the characteristic exponent bifurcates for a value of advance ratio between 0.3 and 0.4 with one of the branches becoming unstable. The stabilizing effect of tip sweep on the second lag mode is also noticeable, results for this case can be found in Ref. [27].

Tip sweep has a relatively minor effect on the stability of the flap and torsion degrees of freedom in forward flight. Results illustrating the influence of sweep on these degrees of freedom are not presented here, due to lack of space, however such results can be found in Ref. 16. Another important effect due to sweep is its influence on the aeroelastic response. Figure 6 shows the torsional response of the tip at an advance ratio $\mu = 0.4$ for the soft-in-plane configuration and for three values of the tip sweep angle Λ(0, 5, and 10°). It is evident from the figure that tip sweep induces a nosedown steady elastic twist, and reduces the amplitudes of the first and second harmonics of the torsional response. Again numerous additional results can be found in Refs. 16 and 27.

An important measure of aeroelastic response, which is relevant for the structural optimization studies which are presented in the next section, is the effect of sweep on the peak-to-peak values of the 4/rev vertical hub shears of a four bladed hingeless soft-in-plane blade.

The calculation of the hub shears is carried out using a direct load integration technique [16] by assuming that the response of the blade is known in the form of Fourier series expansions of the generalized coordinates. The aerodynamic and inertia loads contributions to the root shears are obtained by integration, over the blade span, for the reference blade. The total hub loads are calculated by summing up the contributions from all four blades, after each contribution has been transformed from the rotating to the non-rotating coordinate system. All blades are assumed to be identical. The principal component obtained for a four bladed rotor is the 4/rev component of the vertical hub shears [16].

Figure 7 shows the peak-to-peak value of V_{zpk} of the vertical hub shears as a function of the tip sweep Λ, for four different values of the advance ratio μ. It is evident from the figure that tip sweep may or may not be beneficial for the soft-in-plane configuration, depending on the combination of the advance ratio and sweep angle present. At an advance ratio $\mu = 0.30$ the oscillatory loads rapidly increase with tip sweep. However, at $\mu = 0.40$ tip sweep has a beneficial effect. On the other hand, for the stiff-in-plane configuration tip sweep increases the oscillatory vertical hub shears for all combinations of μ and Λ considered. These results can be found in Refs. 16 and 29.

Based on these results the advance ratio at which the hub shears are minimized, i.e. the objective function in this optimization study, was selected as the vertical hub shears at $\mu = 0.40$.

IV.2. Structural Optimization of Rotor Blades

The basic blade configuration considered in the optimization studies was the soft-in-plane rotor considered in the previous section. The blade precone angle β_p, the root offset e_1 and the offset x_I between the elastic axis and cross sectional center of mass, were all set to zero, unless otherwise stated. For the swept tip configurations, the outermost 10% of the blade is swept. The modal coordinate transformation is based on the six lowest frequency rotating, coupled modes of the blade. For all cases the six modes were: one torsion, two lag, and three flap modes. All blade configurations were modeled using five finite elements, with nodes at 0%; 22.5%; 45%; 67.5%; and 100% of the span. Only selected results are presented here, numerous additional results can be found in Refs. 16 and 29.

Two types of cross sections were considered in this study, namely a single cell, rectangular cross section, and a double cell cross section. Both cross sections are shown in Figure 8. Up to five, and up to nine independent design parameters can be specified for the single cell and the double cell cross section respectively [16]. In this study the cross sectional design parameters are linked in such a way as to reduce the number of independent

design parameters to two, for both single and double cell cross sections. The first independent design variable is the thickness t_1 of all the elements of which both cross sections are composed. The second independent design variable is the chordwise width x_2 for both cross sections. In the single cell cross section the ratio between the width x_2 and the height h_s is kept constant, with $x_2/h_s = 4.5$. In the double cell cross section the internal wall is placed halfway between the leading edge and the rear wall, so that $x_1 = x_2/2$. The outside wall of the double cell cross section has the shape of a NACA 0012 airfoil. The properties of both cross sections are presented in Ref. [16].

Three optimization studies were conducted using the general procedure outlined in the previous section, namely:

1. Optimization of a completely straight blade, having a two-cell cross section. The objective function is the peak-to-peak value of the 4/rev vertical hub shears at an advance ratio $\mu = 0.4$ Because the cross section is not doubly symmetric, the blade generally has nonzero values of the aerodynamic center-elastic axis offset x_A and of the center of gravity-elastic axis offset x_I.

   The design variables are defined at three distinct cross sections of the blade: the root section, the tip section, and the cross section at the 67.5% span, for a total of six independent design variables. The 67.5% station, at which two design variables are defined, is the junction section between the third and the fourth finite element. The blade properties are assumed to vary linearly between two consecutive stations at which the design variables are specified.

2. Optimization of a completely straight blade, having a single cell cross section. As in the previous case, the objective function is the peak-to-peak value of the 4/rev vertical hub shears at an advance ratio $\mu = 0.4$.

   As in Case 1, the design variables are defined at three distinct cross sections of the blade: the root section, the tip section, and the cross section at the 67.5% span, for a total of six independent design variables.

   The cross section is rectangular, therefore doubly symmetric. Because the leading edge masses have not been used in this particular example, the center of gravity and the aerodynamic center are located on the elastic axis of the blade - which is taken to be coincident with the pitch axis. Therefore the associated offsets are equal to zero.

3. Straight blade with a swept tip. The objective function is the peak-to-peak value of the 4/rev vertical hub shears divided by the thrust coefficient C_T, at an advance ratio $\mu = 0.4$. This particular choice of objective function is an attempt to compensate for the inaccuracy of the trim program, which neglects the torsional deformation of the blade, and thus overestimates the thrust that the rotor is actually capable of developing.

   The outermost 10% of the blade is swept, with the sweep angle being a design variable of the optimization procedure. The cross section is rectangular, and therefore the offsets x_I and x_A are equal to zero. The cross sectional design variables are defined as in Case 2. Therefore a total of seven design variables is used in this case.

The initial blade configuration, for all three cases, is the baseline soft-in-plane configuration.

Optimization case 1. The iteration history of the objective function for case 1 is shown in Fig. 9. It should be noted that for all three optimization cases, design n is defined as the design produced at the end of the optimization step n. Step 0 and the first six steps are not true optimization steps; they are required to obtain enough information to build linear approximations to the objective function and behavior constraints. Step 0 is the analysis of the baseline design. In steps 1 through 6 each of the six design variables is perturbed, one at a time. Because the perturbations were relatively small - 1% of the baseline value - the linear approximations obtained at the end of step 6 can be considered as gradients calculated using forward finite difference approximations.

Step 7 is the first true optimization step, and consists of the solution of a linear optimization problem. Move limits were placed on the design variables, which could not change by more than 25% of the baseline value. The optimization continues for three additional steps (8-10). Each new proposed design is analyzed precisely, and used to improve the polynomial approximations to objective function and behavior constraints. The diagonal of the Hessian matrix is built first, as more function evaluations become available. (The term "Hessian" is used in this section with the general meaning of "matrix of coefficients of the quadratic terms of the approximation"). Figure 9 shows that, after reaching a minimum at step 8, the objective function slightly oscillates.

At the constrained optimum of the approximate problem the approximate flap damping constraint for the first flap mode was active. In most helicopter blades the first flap mode tends to be highly damped, and a precise analysis of the proposed design showed that this indeed was the case, and that the precise first flap stability constraint was satisfied. The constraint was therefore reformulated as:

$$\zeta_{F1} - 0.3 < 0 \qquad (41)$$

The subsequent optimization steps were performed with this new form of the constraint, which prevents the approximate constraint from becoming critical. Two more steps (11 and 12) are performed with the relaxed flap constraint. The design of step 12 is a local, unconstrained minimum of the approximate problem. The corresponding blade is such that a reduction of 54.3% is achieved in the objective function, compared with the baseline configuration. The design suggested by the optimizer for step 13 is practically the same as that for step 12. A different design was instead arbitrarily selected for step 13. This design was "close" to that of step 12, and was selected primarily for

the purpose of adding one design to the design data base and try to improve the accuracy of the approximations in the neighborhood of design 12 - with the design of step 13 the full diagonal of the Hessian can be built. Step 14 is the last optimization step, and it produces a value of the objective function that is slightly higher than the minimum step 12. The optimization was arbitrarily stopped at this point. All the designs generated during the optimization were feasible. With the only exception of the damping constraint on the first flap mode at step 10, no behavior constraints were active.

The iteration history on the design variables can be found in Ref. 29 and for the case of conciseness these results are not presented here. The structural optimizer tends to make the structural cross section wider, and therefore stiffer, going from the blade root toward the tip.

Optimization case 2. The iteration history of the objective function for case 2 is shown in Fig. 10. Steps 0 through 6 are not true optimization steps. These steps are required to generate enough designs to construct at least linear approximations to objective function and behavior constraints. The design at step 0 is the baseline blade design. The designs analyzed in steps 1 through 6 are obtained by changing one design variable at a time. Since the change in each variable was equal to 10% of its baseline value, the resulting linear approximations to objective functions and behavior constraints cannot be considered as gradients anymore.

The first true optimization step is step 7, which consists of a linear, constrained optimization problem. A reduction of 37.6% is achieved, compared with the baseline design. In the next step the objective function increases slightly. Because this behavior is somewhat similar to the one observed in case 1, the optimization was arbitrarily concluded at this point, and restarted with a new set of behavior constraints.

The aeroelastic stability constraints used in case 1, and up to this point in case 2, consist of requiring that the blade be aeroelastically stable in hover. It is prudent to require that the optimization processes do not degrade too much the stability of the baseline design. The optimization was thus restarted from step 9 with these more stringent behavior constraints. The aeroelastic constraints of Eq. (39) are reformulated as:

$$g(\vec{D}) = 1 - \frac{\zeta_k}{0.95\zeta_{kB}} \leq 0 \; ; \qquad k = 1,2,\ldots,m \qquad (42)$$

Eq. (42) expresses the requirement that the loss of stability of a given mode should not exceed 5% of the baseline value ζ_{kB}.

The optimization is not restarted with a new calculation of an initial linear approximation. Rather, the previous designs are reused to provide the initial approximation for the new case. While designs 0 through 8 were all feasible with respect to the old set of behavior constraints some of these designs are now infeasible with respect to the tightened aeroelastic stability constraints. In particular, design 8, which becomes the initial design for the second phase of this optimization, is infeasible.

The first design produced by the optimizer with the new set of constraints is feasible with respect to the approximate behavior constraints. When this design is analyzed precisely, it proves to be infeasible with respect to the exact behavior constraints. The successive design (step 10) is feasible with respect to both the approximate and the exact behavior constraints. The next design (step 11) is again feasible with respect to the approximate, but not the exact behavior constraints. In steps 9 through 11 the objective function is constantly at a value higher than the baseline value, and does not show any signs of convergence to the optimum. In other words the optimizer does not seem to be able to produce a feasible design that improves on the baseline design - which obviously satisfies the new constraint equations, Eq. (42).

The apparently erratic behavior of the objective function required a reconsideration of the optimization strategy which, starting from step 14, was modified as follows:

1. At each optimization step, take as the baseline design $\vec{D}_0$ the design with the lowest value of the objective function, whether or not that design is the latest analyzed, and whether or not that design is feasible. Impose relatively tight move limits on the design variables, for example allowing a maximum change of 10% of the baseline value.

2. If the new design generated by the optimizer has a lower value of the objective function, use it as the starting point for the next optimization step with the design with the lowest value of the objective function. Tighten the move limits further.

3. When a good design is obtained, use it as the starting point for the next optimization step, and progressively widen the move limits.

4. If the design with the lowest value of the objective function is infeasible, and the optimizer consistenly fails to produce a design that is both feasible, and with a value of the objective function lower than that of the initial design, restart the optimization from the initial design. Do not discard any of the previous designs, unless enough function evaluations have already been performed to construct a complete quadratic equation.

The new strategy is applied starting from step 14, shown in Fig. 10. The starting design is design 2, which is infeasible and has the lowest value of the objective function. Move limits are placed on the design variables. The maximum allowable change is 10% of the values of design 2. The design produced by CONMIN is still infeasible, but already shows a large decrease in the objective function. The next step (step 15) again uses design 2 as the starting design. The same move limits as in the previous step are imposed. Design 15 is now feasible, although the objective function has increased. Step 15 again starts from design 2, but the move limits are tightened. A maximum

change of only 5% in the value of the design variables is now allowed, with respect to design 2. The design produced by the optimizer has a value of the objective function which is still higher than that of design 2, but lower than the baseline value of design 0. Furthermore, design 16 is feasible whereas design 2 was not. Design 16 is constrained by the move limits. The reduction in the peak-to-peak value of 4/rev vertical hub shears of 16.6% compared with the baseline value. Thus the imposition of the tightened aeroelastic constraints reduces the gains in the objective function by more than 50%.

This design is used as the starting design for step 17. The move limits are widened from 5% to 10%. The design produced by CONMIN is so close to that of step 15 that a new precise analysis is not performed - for this reason step 17 is not included in Fig. 10. The design is now constrained by the approximate aeroelastic constraints. The first lag, second flap, and second flap constraints are active. The second lag constraint is slightly violated, but it remains within the narrow numerical band that straddles the exact value of the constraint - constraints are usually defined in CONMIN as narrow strips instead of strictly as lines [25]. The side constraints are no longer active.

Design 17 is at least a local minimum for the approximate problem. It is not necessarily a local minimum for the exact problem. Whether or not this is the case depends the quality of the approximations to objective function and behavior constraints.

Optimization case 3. Figure 11 shows the iteration history of the objective function for case 3, which is the peak-to-peak value of the 4/rev vertical hub shears divided by the thrust coefficient, c_T. The tightened aeroelastic constraints of Eq. (42) are enforced.

Design 0 is the baseline soft-in-plane straight blade configuration. The first seven steps are not true optimization steps. As in cases 1 and 2, they provide enough precise values of the objective function and behavior constraints to build at least a linear approximation of objective function and constraints. In the designs 1 through 7 each of the seven design variables is perturbed, one at a time. Design 7 is the only swept blade design. Designs 0 through 6 are straight blade designs, and are identifical to the corresponding designs of case 2. Thus these designs are not reanalyzed, and the values obtained in case 2 are reutilized. The swept tip blade of design 7 is one of the blade configurations analyzed to derive the results of Figure 11, and need not be recalculated.

Thus the optimization process of case 3 begins without the need for any precise analyses, in the sense that the eight precise analyses required to start the procedure were already available from previous parts of this study, and could be directly reutilized. The ability to make use of previously analyzed designs, even if not very close to the expected optimum in the design space of the current problem, is one of the most important features of the optimization algorithm used in this study.

The first true optimizaiton step - step 8 - produces a design with a reduction of 27.2% of the objective function with respect to the baseline straight blade. This also corresponds to a reduction of 14.5% with respect to the best swept tip design obtained without applying formal optimization techniques, that is design 7. When analyzed precisely, the design proves feasible, with no constraints active. Compared with the final result of case 2, in which the blade is straight, the use of tip sweep as an additional design variable allows a further reduction of the objective function of almost 10%.

The next two steps (9 and 10) produce much higher values of the objective function. Starting from step 11 the "modified" strategy previously outlined is employed. The next two steps (11 and 12) provide considerable reductions of the objective function, but the best design is still design 8. The optimization is arbitrarily stopped at this point, both for cost reasons, and because the design appears to converge towards design 8.

The iteration histories of the thickness t_1, the chordwise extension of the spar, and the tip sweep angle Λ are shown in Figs. 12, 13 and 14, respectively. The tip sweep angle corresponding to the best design is $\Lambda = 9°$.

Computational requirements. All the results presented in this study were obtained on an IBM 3090-200 computer. Each precise aeroelastic analysis required three or four iterations of quasilinearization [16]. Each iteration of quasilinearization required 80-110 CPU seconds for a straight blade and 140-180 CPU seconds for a swept tip blade. Because a variable step, Adams-Bashforth technique was used to integrate the equations of motion [27], the exact CPU time required to complete an iteration of quasilinearization was problem dependent.

The remaining portions of a complete optimization step, namely the calculation of the cross sectional properties of the blade, the calculation of the vertical hub shears from the aeroelastic response of the blade, the derivation of the polynomial approximations to objective function and behavior constraints, and the solution of the approximate constrained optimization problem, required an average total of 1-2 CPU seconds.

V. Concluding Remarks

This paper presents a fairly comprehensive model which is capable of simulating the aeroelastic stability and response behavior of helicopter rotor blades with swept tips. Furthermore the paper also presents an effective technique for the structural optimization of rotor blades with straight and swept tips, subject to aeroelastic constraints. The principal conclusions of the paper are briefly listed below.

1. Tip sweep has a powerful influence on the dynamic behavior of the hingeless rotor blade. No general conclusions can be drawn concerning whether given amounts of tip sweep will stabilize or destabilize a given blade configuration, because its effects will depend on

other blade design parameters, such as precone and the combination of blade fundamental frequencies. Therefore, the beneficial effects of sweep can be best exploited if tip sweep is included, as a design parameter, in the early stages of the dynamic design of the rotor.

2. The aeroelastic instabilities induced by tip sweep are associated with frequency coalescence. Such instabilities are strong and they are not eliminated by the addition of small amounts of structural damping. The types of modes that coalesce depend on the blade design. Therefore, only fully coupled flap-lag-torsion analyses should be used for the prediction of the aeroelastic stability of the blade.

3. When frequency coalescence does not occur, tip sweep is usually stabilizing. In particular, small amounts of tip sweep can remove the first lag mode instability, characteristic of stiff-in-plane hingeless rotors in forward flight.

4. The optimimum design procedure described in this study is very efficient, and can produce improved designs with a very limited number of precise analyses. The method of constructing the approximate problem is such that previously conducted aeroelastic analyses can be reused in a new optimization problem.

5. The results of the optimization are quite sensitive to the aeroelastic stability margins required of the blade. In the optimization of case 2, changing the aeroelastic stability constraints from the requirement that the blade be stable in hover, to requiring that the stability margins be maintained during the course of the optimization, reduced the gains in n/rev vibration level reduction by more than 50%.

6. The introduction of tip sweep can reduce the n/rev vertical hub shears beyond the level that can be obtained by just modifying the mass and stiffness distributions of the blade.

VI. Acknowledgement

This research was funded by NASA grant NAG 2-226, NASA Ames Research Center, Moffett Field, CA. The support of grant monitor, Dr. H. Miura, is gratefully acknowledged.

VI. References

1. Desopper, A., Lafon, P., Ceroni, P., and Phillipe, J.J., "10 Years of Rotor Flows Studies at ONERA - State of the Art and Future Studies", 42nd Annual Forum of the American Helicopter Society, Washington, D.C., June 1986.

2. Thibert, J.J. and Philippe, J.J., "Etudes de Profils et D'Extremites de Pale D'Helicoptere," AGARD Conference Proceedings, No. 334, May 1982, pp. 3.1-3.14.

3. Philippe, J.J., and Vuillet, A., "Aerodynamic Design of Advanced Rotors with New Tip Shapes", 39th Annual Forum of the American Helicopter Society, St. Louis, Missouri, May 1983.

4. Tarzanin, F.J., and Vlaminck, R.R., "Investigation of the Effect of Blade Sweep on Rotor Vibratory Loads", NASA CR-166526, October 1983.

5. Friedmann, P.P., "Recent Trends in Rotary-Wing Aeroelasticity", Vertica, Vol. 11, No. 1/2, 1987, pp. 139-170.

6. Rosen, A., and Rand, O., "A General Model of the Dynamics of Moving and Rotating Rods", Computers and Structures, Vol. 21, No. 3, 1985, pp. 543-561.

7. Rosen, A., and Rand, O., "A Nonlinear Model of Aeroelastic Behavior of Rotor Blades in Forward Flight", Vertica, Vol. 10, No. 1, 1986, pp. 9-21.

8. Young, D.K., Tarzanin, F.J., and Kunz, D., "Use of Blade Sweep to Reduce 4/Rev Hub Loads", Proceedings of the 43rd Annual Forum of the American Helicopter Society, St. Louis, Missouri, May 1987.

9. Walker, W.R., and Hatch, C., "Pitch-Flap Flutter Instability of a Swept-Tip Model Rotor Blade", Proceedings of the Thirteenth European Rotorcraft Forum, Paper No. 6.12, Arles, France, September 1987.

10. Friedmann, P.P., "Application of Modern Structural Optimization to Vibration Reduction in Forward Flight", Vertica, Vol. 9, No. 4, 1985, pp. 363-373.

11. Miura, H., "Application of Numerical Optimization Methods to Helicopter Design Problems - A Survey", Vertica, Vol. 9, No. 2, 1985, pp. 141-154.

12. Schmit, L.A., Jr., and Miura, H., "Approximation Concepts for Efficient Structural Synthesis", NASA CR-2552, 1976.

13. Friedmann, P.P., and Shanthakumaran, P., "Optimum Design of Rotor Blades for Vibration Reduction in Forward Flight", Journal of the American Helicopter Society, Vol. 29, No. 4, October 1984, pp. 70-80.

14. Shamie, J. and Friedmann, P.P., "Effect of Moderate Deflections on the Aeroelastic Stability of a Rotor Blade in Forward Flight", Paper No. 24, 3rd European Rotorcraft Forum, Aix-en-Provence, France, September 1977.

15. Celi, R. and Friedmann, P.P, "Use of an Implicit Formulation Based on Quasilinearization for the Aeroelastic Response and Stability of Rotor Blades in Forward Flight", Paper No. 87-0921-CP, AIAA Dynamics Specialist Conference, Monterey, Calif., April 1987 (to appear in the AIAA Journal).

16. Celi, R., "Aeroelasticity and Structural Optimization of Helicopter Rotor Blades with Swept Tips", Ph.D. Dissertation, Mechanical, Aerospace and Nuclear Engineering Department, University of California, Los Angeles, October 1987.

17. Straub, F.K. and Friedmann, P.P., "Application of the Finite Element Method to Rotary Wing Aeroelasticity", NASA CR-165854, February 1982.

18. Panda, B., "Technical Note: Assembly of Moderate-Rotation Finite Elements Used in Helicopter Rotor Dynamics", Journal of the American Helicopter Society, Vol. 32, No. 4, October 1987, pp.

19. Friedmann, P.P., and Kottapali, S.B.R., "Coupled Flap-Lag-Torsional Dynamics of Hingeless Rotor Blades in Forward Flight", Journal of the American Helicopter Society, Vol. 27, No. 4, October 1982, pp. 28-36.

20. Chattopadhyay, A., and Walsh, J., "Minimum Weight Design of Rectangular and Tapered Helicopter Rotor Blades with Frequency Constraints", Proceedings of the Second International Conference on Rotorcraft Basic Research, College Park, Maryland, February 1988.

21. Pritchard, J.L., and Adelman, H.M., "Optimal Placement of Tuning Masses for Vibration Reduction in Helicopter Rotor Blades", Proceedings of the Second International Conference on Rotorcraft Basic Research, College Park, Maryland, February 1988.

22. Weller, W.H., and Davis, M., "Experimental Demonstration of Helicopter Blade Designs Optimized for Minimum Vibration", Proceedings 44th Annual Forum of the American Helicopter Society, Washington, D.C., June 1988.

23. Vanderplaats, G.N., "Approximation Concepts for Numerical Airfoil Optimization", NASA Technical Paper 1370, March 1979.

24. Vanderplaats, G.N., "Numerical Optimization Techniques for Engineering Design, With Applications", McGraw-Hill Book Co., 1984, pp. 211-215.

25. Vanderplaats, G.N., "CONMIN - A FORTRAN Program for Constrained Function Minimization; User's Manual", NASA TMX-62,282, August 1973.

26. Prouty, R.W., "Helicopter Performance, Stability and Control", PWS Publishers, Boston, 1986.

27. Celi, R., and Friedmann, P.P., "Aeroelastic Modeling of Swept Tip Rotor Blades Using Finite Elements", Journal of the American Helicopter Society, Vol. 33, No. 2, April 1988, pp. 43-52.

28. Friedmann, P.P., "Influence of Modeling and Blade Parameters on the Aeroelastic Stability of a Cantilevered Rotor Blade", AIAA Journal, Vol. 15, No. 2, February 1977, pp. 149-158.

29. Celi, R. and Friedmann, P.P., "Structural Optimization with Aeroelastic Constraints of Rotor Blades with Straight and Swept Tips", AIAA Paper 88-2297, Proceedings of AIAA/ASME/ASCE/AHS 29th Structures, Structural Dynamics and Materials Conference, Part 2, pp. 668-680, Williamsburg, Virginia, April 1988.

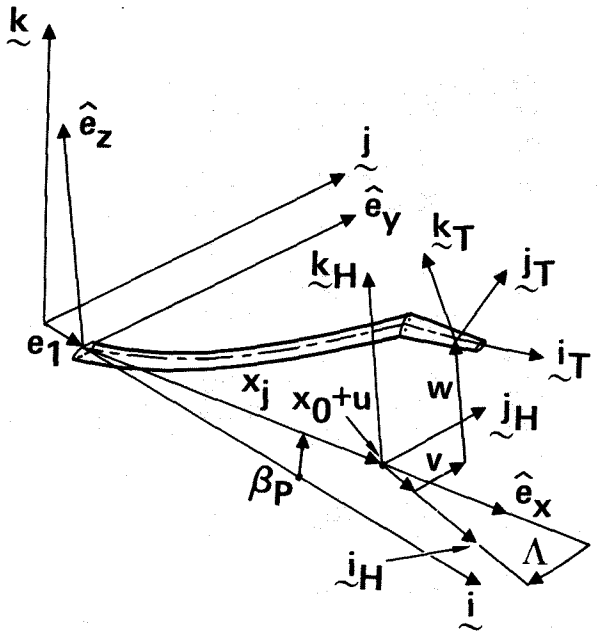

Figure 1: Blade geometry and coordinate systems.

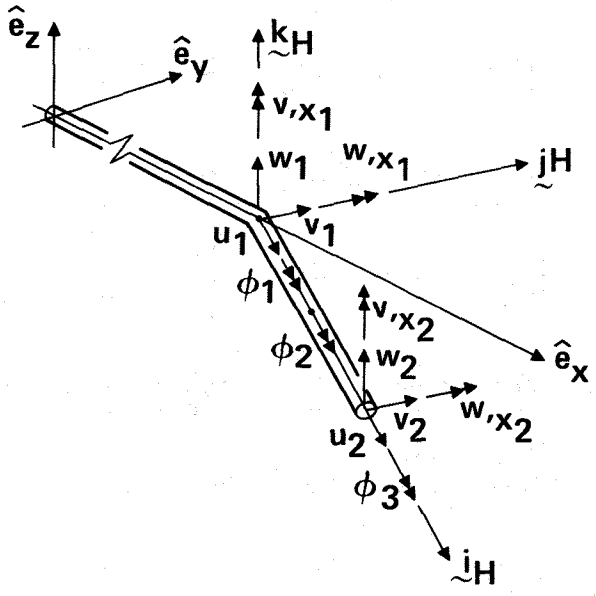

Figure 2: Tip element-local coordinate system and degrees of freedom.

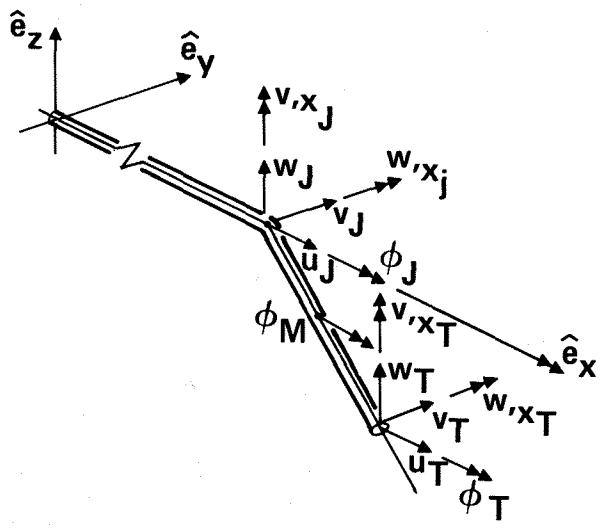

Figure 3: Tip element-global coordinate system and degrees of freedom.

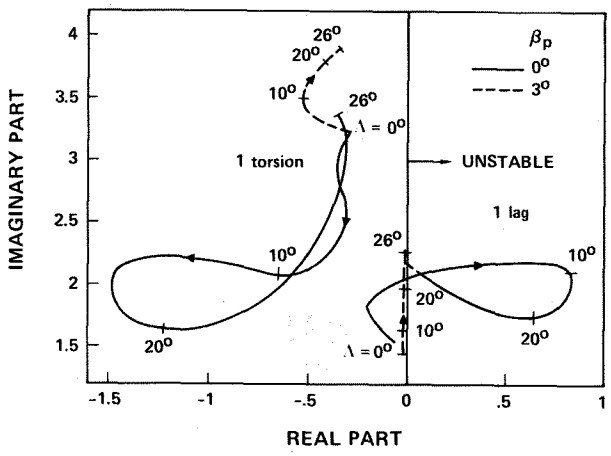

Figure 4: Root locus of first torsion and first lag hover stability eigenvalues, for stiff-in-plane blade configuration and tip length ℓ_T = 0.10R.

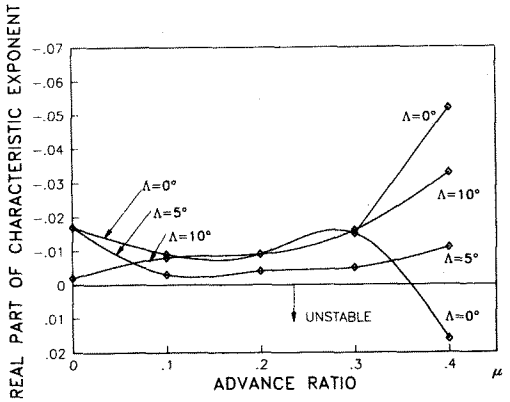

Figure 5: Effect of sweep on the real part of the characteristic exponent of the first lag mode. Stiff-in-plane blade configuration. Tip length ℓ_T = 0.1R. Precone β_p = 3°.

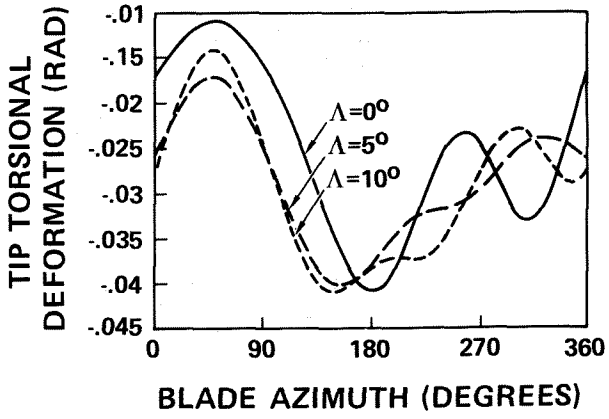

Figure 6: Effect of tip sweep angle on the torsional response, at the blade tip, for the soft-in-plane blade configuration. Advance ratio μ = 0.40 and tip length ℓ_T = 0.10R.

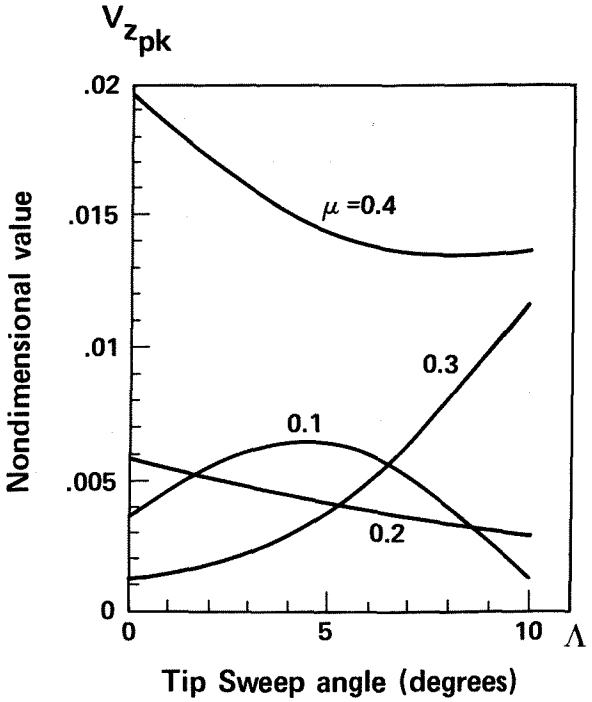

Figure 7: Effect of tip sweep on the peak-to-peak value of the vertical hub shears for the soft-in-plane blade configuration.

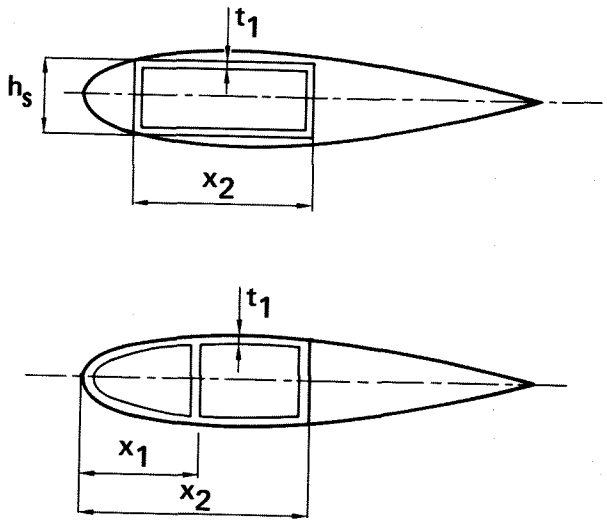

Figure 8: Single and double cell cross sections.

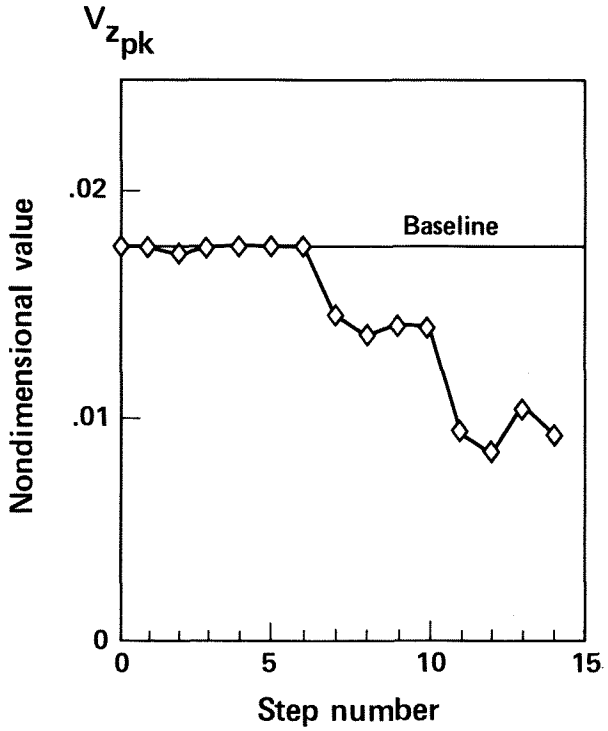

Figure 9: Case 1 - iteration history of the objective function.

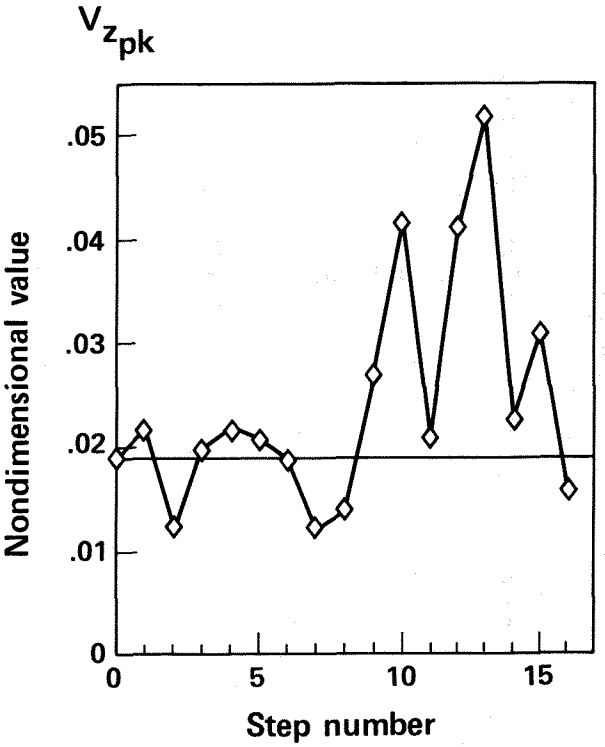

Figure 10: Case 2 - iteration history of the objective function.

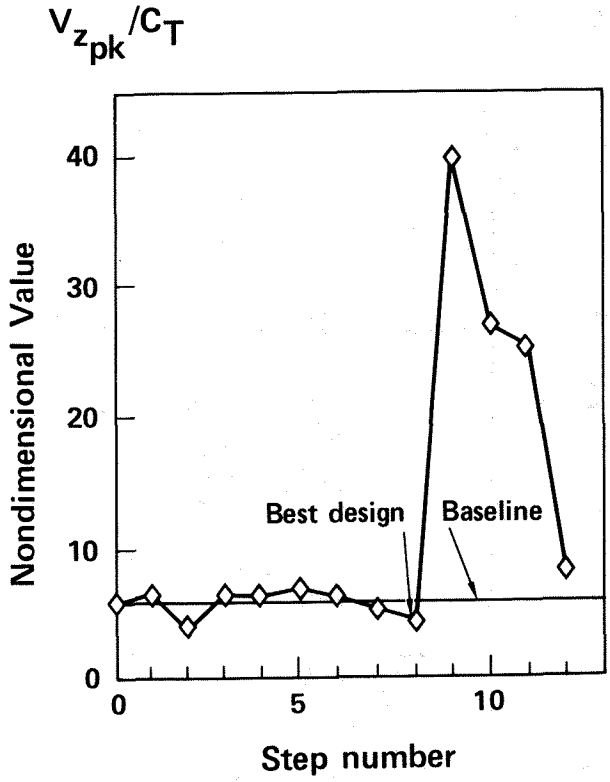

Figure 11: Case 3 - iteration history of the objective function.

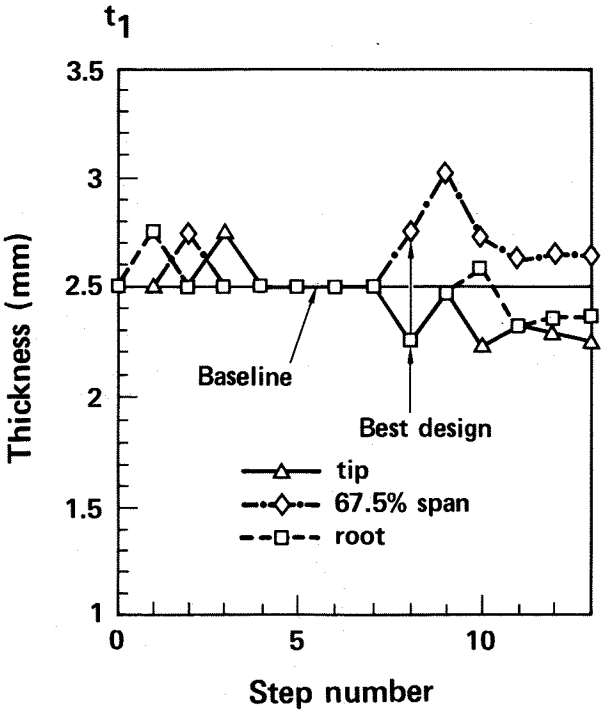

Figure 12: Case 3 - iteration history of the thickness t_1.

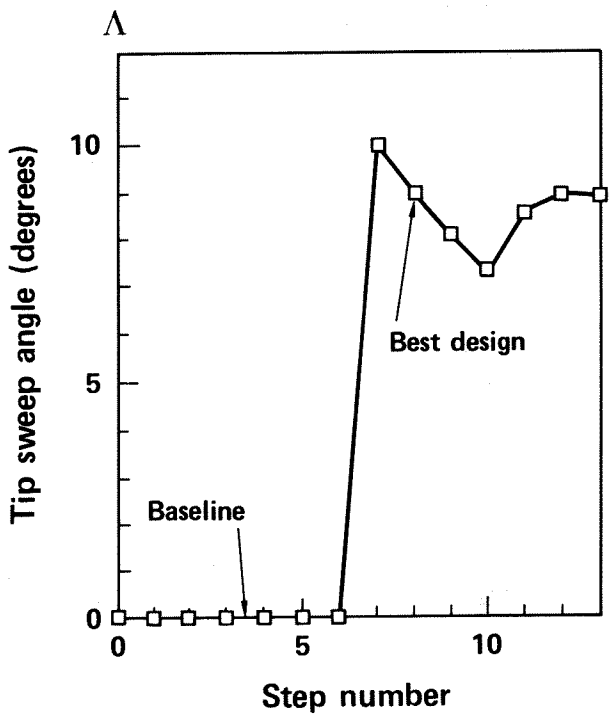

Figure 14: Case 3 - iteration history of the tip sweep angle Λ.

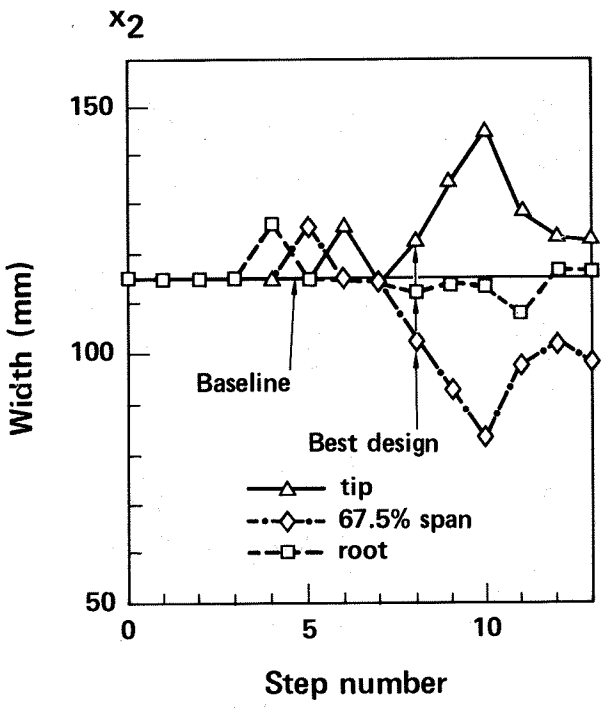

Figure 13: Case 3 - iteration history of the chordwise width x_2.